

Absolute and “upstream” convective instabilities in plane Couette-Poiseuille flow

Kirthy K. Srinivas¹ and Sourabh S. Diwan¹†

¹Department of Aerospace Engineering, Indian Institute of Science, Bengaluru 560012, India

(Received xx; revised xx; accepted xx)

Here we report some interesting new features of the spatio-temporal instability of the incompressible plane Couette-Poiseuille flow (CPF). First of all, this flow represents the first instance of a “non-inflectional” absolute instability, within constant-viscosity formulation, which is triggered when one of the plates moves opposite to the bulk motion. More strikingly, with further increase in the negative plate motion, the absolute instability (AI) transitions to an “upstream” convective instability (CI^-), wherein an unstable wave packet moves opposite to the direction of the bulk flow. Thus, the CPF exhibits a unique $CI^+ \rightarrow AI \rightarrow CI^-$ transition, for a given Reynolds number (Re), where CI^+ denotes the commonly-observed case of a “downstream” convective instability. This type of transition has not been reported for other known examples of absolutely unstable flows. We compute the leading and trailing edge velocities for an amplifying wave packet and find that, for the plane Poiseuille flow, both these velocities approach zero as $Re \rightarrow \infty$. As a result, at high Re , even the slightest of negative plate motions is sufficient to trigger AI and subsequently CI^- , as observed for the CPF. The wave-packet dispersion first increases with Re , followed by a decrease, which points to a peculiar “dual” role of viscosity in sustaining AI in the CPF, namely, viscosity promotes sustenance of AI at moderate Reynolds numbers but suppresses it at low and high Reynolds numbers. These results can be well understood within the Ginzburg-Landau framework, and therefore can be expected to have a wider applicability.

1. Introduction

One of the important developments in the modern theory of hydrodynamic stability has been the classification of instabilities into convective and absolute instability (Huerre & Monkewitz 1990; Chomaz 2005). The convectively unstable flows behave as noise amplifiers, whereas the absolutely unstable flows exhibit an intrinsic oscillator behaviour; the latter can also lead to a “global” instability affecting the entire flow domain (Chomaz 2005).

The prototypical examples of absolutely unstable flows include a mixing layer, a near-wake and a heated jet (Huerre & Monkewitz 1990); there have also been several other types of flow, such as separated flows (Alam & Sandham 2000), the rotating-disk boundary layer (Lingwood 1995), the Batchelor vortex (Olendraru & Sellier 2002) etc., in which absolute instability has been observed. It is worth noting that these and other known cases of absolutely unstable flows contain an inflection point in the base velocity profiles and are therefore governed primarily by the inviscid instability mechanism (Huerre & Monkewitz 1990; Drazin & Reid 2004). On

† Email address for correspondence: sdiwan@iisc.ac.in

the other hand, the non-inflectional flows such as the Blasius boundary layer, the channel flow and the plane Couette flow, which are governed by the viscous instability mechanism (Drazin & Reid 2004), have been found to be convectively unstable (Huerre & Monkewitz 1990). There exist more complex situations involving absolute instability, such as a channel flow with viscosity stratification (Govindarajan & Sahu 2014), but the velocity profile for this case is found to be inflectional. To the best of our knowledge, the onset of absolute instability in a *non-inflectional* flow has not been reported so far. In this work, we show that the plane Couette-Poiseuille flow, within the incompressible constant-viscosity framework, provides the first instance of such a “viscous non-inflectional” absolute instability. Interestingly, this flow also exhibits an “upstream” convective instability.

The plane Couette-Poiseuille flow (CPF) is obtained by applying favourable pressure gradient to a fluid between two plane parallel plates (Poiseuille component of the flow) and setting one of the plates in motion (Couette component of the flow), and is given by

$$U(y) = \frac{\lambda}{2}(1+y) + (1-y^2) \quad \text{with} \quad \begin{array}{l} y = -1, \quad U = 0 \\ y = +1, \quad U = \lambda \end{array} \quad (1.1)$$

where y is the wall normal coordinate, U is the streamwise velocity and $\lambda = U_c/U_p$ is ratio of the upper plate speed, U_c and the Poiseuille component of centreline velocity, U_p ; see figure 1(a). Here y is non-dimensionalized by the half-width of the channel, b .

The plane Poiseuille flow (PPF), obtained by setting $\lambda = 0$ in (1.1), has been studied extensively as a prototype of linear viscous instability (Drazin & Reid 2004; Nishioka *et al.* 1975), as it is a strictly parallel flow that is an exact solution of the Navier-Stokes equations (as is the CPF). Deissler (1987) carried out a spatio-temporal analysis of the PPF (which is the only reported study on the topic) and showed that this flow is convectively unstable at all Reynolds numbers. Interestingly, he reported that the trailing edge velocity of the wave packet decreases with increasing Reynolds number, but the implications of this finding was not explored further (Deissler 1987). This observation, which sets the stage for the present investigation, is found to have far-reaching consequences for the stability of the CPF.

The linear and nonlinear stability characteristics of the CPF have been investigated in the past, both theoretically/numerically (Potter 1966; Cowley & Smith 1985; Kumar & Walton 2019; Kirthy K. & Diwan 2021) as well as experimentally (Klotz *et al.* 2017). An important result from the linear stability analysis (Potter 1966) is that the motion of the plate (either in the positive or negative direction) makes the CPF more stable as compared to PPF and for $|\lambda| > 0.7$, there is a complete stabilization of the flow. A physical explanation for this observation was given by Kirthy K. & Diwan (2021) in terms of emergence of a region of negative production with an increase in $|\lambda|$; they also carried out a detailed characterization of eigenvalues for $\lambda > 0$ and $\lambda < 0$. Despite these studies, the effect of plate motion on the spatio-temporal behaviour of the CPF has not been reported so far. Here we show that the negative plate speed (i.e. opposite to the Poiseuille component of the flow), although having a slight stabilizing effect on the spatial growth rates, has a profound influence on the convective/absolute character of the CPF - even the slightest reverse flow induced by the moving plate is sufficient to trigger absolute instability, provided the Reynolds number Re is large enough. Here $Re = U_p b/\nu$, ν being the kinematic viscosity. As the negative plate speed increases, the absolute instability is realized at increasingly lower values of Re . Another striking feature we observe is that the absolute instability in the CPF is sustained only for a certain range of $\lambda (< 0)$ and Re . For λ exceeding this range (for a given Re), the flow reverts back to being convectively unstable; the direction of the wave-packet propagation, however, is opposite to the bulk fluid motion, i.e., in the upstream direction.

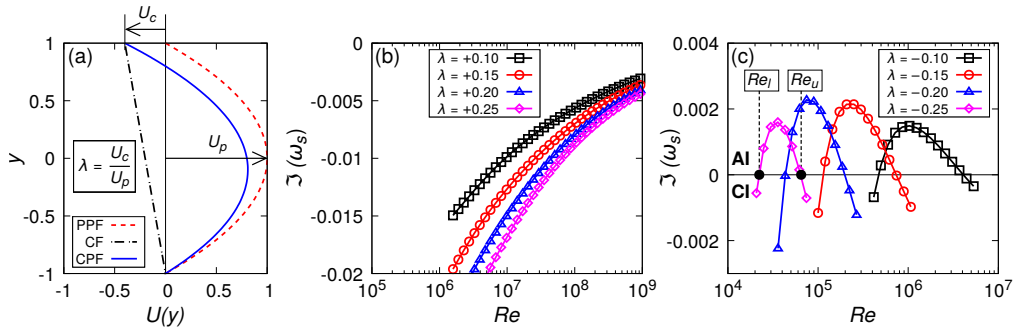


Figure 1: (a) The base velocity profile for the CPF. CF indicates the Couette flow component. (b) The absolute growth rate $\Im(\omega_s)$ as a function Re for $\lambda > 0$, and (c) $\lambda < 0$.

2. Spatio-temporal stability analysis of Couette-Poiseuille flow

The viscous spatio-temporal problem for the evolution of infinitesimal disturbances on a parallel base flow is governed by the Orr-Sommerfeld (O-S) equation (Drazin & Reid 2004). For the present base flow (1.1) the O-S equation is solved using the Chebyshev pseudo-spectral method. The disturbances are represented as Fourier modes - $v(x, y, t) = \hat{v}(y)e^{i(\alpha x - \omega t)}$, where x is the streamwise coordinate, t is time, v is the perturbed wall normal velocity, \hat{v} is the complex eigenfunction, and α and ω , respectively, are the complex (streamwise) wavenumber and frequency. Solving the discrete form of the O-S equation (Kirthy K. & Diwan 2021) results in a dispersion relation of the form $\omega = \omega(\alpha, Re)$, from which the convective/absolute nature of instability is determined using the Briggs-Bers criterion (Briggs 1964; Huerre & Monkewitz 1985). This necessitates locating the saddle point of the dispersion relation, ω_s , which is done numerically using the procedure suggested by Deissler (1987). Our algorithm involves starting with an initial guess (α_o, ω_o) for the saddle point and fitting a complex quadratic to the function $\omega(\alpha)$ using the points $[\omega(\alpha_o), \omega(\alpha_o + \Delta\alpha_o), \omega(\alpha_o - \Delta\alpha_o)]$. By enforcing $\left(\frac{d\omega}{d\alpha}\right) = 0$, we obtain a new value for α_o which serves as the next guess for the saddle point. This iteration is carried out till the location of the saddle point is calculated to a desired degree of accuracy. For the present work, the eigenvalue computations have been validated against existing results for the PPF (Schmid & Henningson 2012) and the CPF (Potter 1966); see Kirthy K. & Diwan (2021). The results from the saddle-point computation have been validated against the data of Deissler (1987); see supplementary figure S1.

2.1. Absolute and “upstream” convective instabilities

Figures 1(b) and 1(c) plot the imaginary part of the saddle point, $\Im(\omega_s)$ (which is the temporal growth rate associated with ω_s), as a function of Re , respectively, for $\lambda > 0$ and $\lambda < 0$. We find that for $\lambda \in (0, 0.7)$ and $Re > Re_c$ (Re_c being the critical Reynolds number), the CPF is convectively unstable, i.e., $\Im(\omega_s) < 0$ (figure 1b), which is consistent with Deissler’s result for $\lambda = 0$ (Deissler 1987). On the other hand, for $\lambda < 0$ (and > -0.2924 ; see figure 2) and for a certain range of Re , the flow is found to be absolutely unstable, i.e., $\Im(\omega_s) > 0$, as seen from figure 1(c). Another interesting observation from figure 1(c) is that, for a given λ , the absolute instability (AI) turns back into convective instability (CI) beyond a particular Re . Thus, the CPF is seen to undergo $CI \rightarrow AI \rightarrow CI$ transitions with increase in Re ; the first transition happens at Re_l and the second at Re_u ; figure 1(c). As λ decreases from -0.1 to -0.25 , both Re_l and Re_u go on decreasing (figure 1c). For a given $\lambda < 0$, the absolute growth rate exhibits a maximum, denoted as $\Im(\omega_s)_{max}$, at the Reynolds number denoted as Re_{max} .

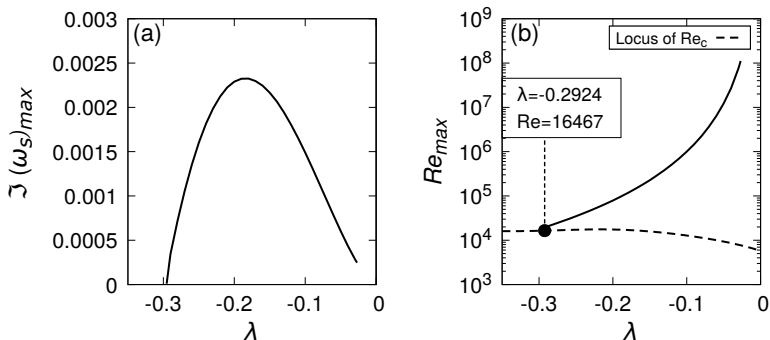


Figure 2: (a) Variation of the maximum absolute growth rate, $\Im(\omega_s)_{max}$, (for a given λ) as a function of λ for the CPF. (b) Variation of the Reynolds number corresponding to the maximum absolute growth rate, Re_{max} , as a function of λ .

Figure 2(a) shows that as λ becomes more negative, the (maximum) absolute growth rate first increases and then decreases, reaching zero at $\lambda \approx -0.3$ ($\lambda = -0.2924$ to be precise). For a more negative λ , $\Im(\omega_s)_{max} < 0$, implying transition to a convective instability (Huerre & Monkewitz 1985). Thus absolute instability is realized for the CPF only for $-0.2924 < \lambda < 0$. Interestingly, at $\lambda = -0.2924$, $Re_{max} = Re_c$ and as $\lambda \rightarrow 0$, $Re_{max} \rightarrow \infty$ (figure 2b). More comments on this behaviour will be made in relation to figure 4.

To explore these characteristics further, we plot the spatial branches (ω real) for $\lambda = -0.25$ in figure 3 for four different values of Re . Here α^+ represents the downstream travelling branch and α^- the upstream branch. The identity of upstream and downstream travelling branches has been confirmed by taking a contour in the complex ω plane above all the unstable temporal modes. This results in a separation of spatial branches into the lower and upper half α planes (Huerre & Monkewitz 1985). For $x > 0$ (i.e., the direction of bulk motion), the contour is closed in the upper half α plane and, for $x < 0$, in the lower half of α plane (supplementary figure S2). For $Re < Re_l$, the amplifying spatial branch is α_I^+ (figure 3) which advects in the direction of the bulk flow. This is the well-understood case of “downstream” convective instability (CI^+), exhibited by a variety of other flows (Huerre & Rossi 1998). For $Re > Re_u$, however, the spatial branches move into the upper half of the α -plane and for this case, α_{II}^- becomes the amplifying branch (figure 3). Thus, for $Re > Re_u$, the unstable wave packet travels upstream, i.e., opposite to the bulk motion, exhibiting an “upstream” convective instability (CI^-). These features seen for $\lambda = -0.25$ are also observed for the other values of λ included in figure 1(c). This is shown in supplementary figure S3, in which the movement of the saddle point (α_s, ω_s) is tracked in the complex α and ω planes for $\lambda = \pm 0.1, \pm 0.15, \pm 0.2$, and ± 0.25 . These results imply that the transitions between CI and AI seen in figure 1(c) are of the form $CI^+ \rightarrow AI \rightarrow CI^-$, and these are observed for the entire range of λ for which the CPF is absolutely unstable, i.e., $\lambda \in (-0.2924, 0)$. This is evident from the parametric plot presented in figure 4(a).

As seen earlier (figure 1c), for a given λ , Re_l and Re_u represent the CI–AI transition points and are marked in figure 4(a). For $\lambda = -0.2914$, below which AI is not present, Re_l and Re_u coincide with each other and are equal Re_c (figure 2b). Note that the $CI^+ \rightarrow AI \rightarrow CI^-$ transitions are also observed at a given Re as λ becomes more negative (figure 1c), with λ_l and λ_u representing the transition points, as shown in figure 4(a). Thus, for the CPF, the AI can be sustained only for a certain range in λ and Re , namely, $\lambda \in (-0.2924, 0)$ and $Re \in (Re_l, Re_u)$, resulting in a “pocket” of absolute instability; the ranges in λ and

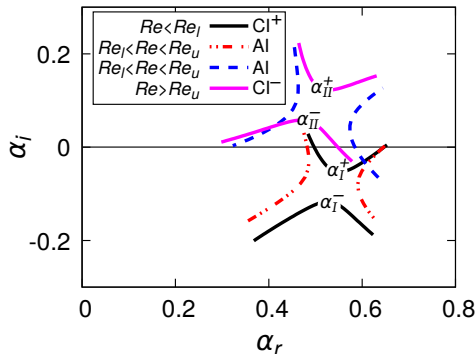


Figure 3: Spatial branches for $\lambda = -0.25$ exhibiting the $CI^+ \rightarrow AI \rightarrow CI^-$ transitions. The four Reynolds numbers used are 2.2×10^4 ($Re < Re_l$), 2.3×10^4 , 5×10^4 ($Re_l < Re < Re_u$) and 7×10^4 ($Re > Re_u$). Note that the branches corresponding to AI do not represent physically meaningful spatial branches as they do not satisfy causality (Huerre & Monkewitz 1990); they are included here to track the movement of the saddle point from the lower to upper α planes.

Re for which AI is realized are plotted in figures 4(b) and (c) respectively. For a given λ , the pocket of AI divides the convectively unstable region into two parts - CI^+ region for $Re \in (Re_c, Re_l)$, and CI^- region for $Re \in (Re_u, \infty)$ (figure 4a). A pocket of AI surrounded by a region of CI was also observed for the instability of the Batchelor vortex (Olendraru & Sellier 2002); however the direction of propagation of CI for this flow was always in the direction of the bulk (axial) flow. The “upstream” convective instability, therefore, seems to be a unique feature of the CPF. Interestingly, this upstream convective instability is observed for any $\lambda < 0$ (and > -0.7), provided $Re > Re_u$; for $\lambda \in (-0.7, -0.2924)$, there exists one continuous CI^- region for $Re > Re_c$ (figure 4a). Thus, for $\lambda \in (-0.7, -0.2924)$, the only modal instability possible for the CPF is CI^- , with the wave packet moving opposite to the bulk motion. (Note that the average velocity for the CPF is $\left(\frac{\lambda}{2} + \frac{2}{3}\right)$ (1.1), which is greater than zero for the entire range of unstable $\lambda \in (-0.7, 0)$.)

Another interesting observation from figure 4(a) is that even for *arbitrarily small* negative values of λ , the CPF exhibits regions of AI and CI^- , although at very high values of Re . Note that the limit of Re_l and Re_u as $\lambda \rightarrow 0$ does not exist, since for $\lambda = 0$, the flow (i.e., the PPF) exhibits only CI^+ (Deissler 1987). As λ becomes more negative for the CPF, Re_l and Re_u drop significantly and approach Re_c as $\lambda \rightarrow -0.2924$ (figure 4a). Therefore, it should be possible to realize AI and CI^- in the CPF in physical situations at moderate plate speeds, provided the background disturbance levels are sufficiently low to enable modal growth. No such instance has been reported in the literature to our knowledge.

2.2. Wave-packet propagation and dispersion

The surprisingly rich behaviour exhibited by the CPF, with regard to the AI-CI transitions, warrants a further investigation. It is well known that, the primary instability mechanism in the CPF, which has a non-inflectional profile, is viscous in character (Drazin & Reid 2004). However, the role viscosity plays in promoting and sustaining absolute instability for this flow has not received attention in the literature. To understand this aspect better, we make a Galilean transformation of the observer frame of reference to $x = x_0 - Vt$ (Deissler 1987), where x_0 represents the laboratory reference frame, and V is the observer speed; see section 2.3 for a discussion on an “objective” frame of reference for the CPF. We then proceed to

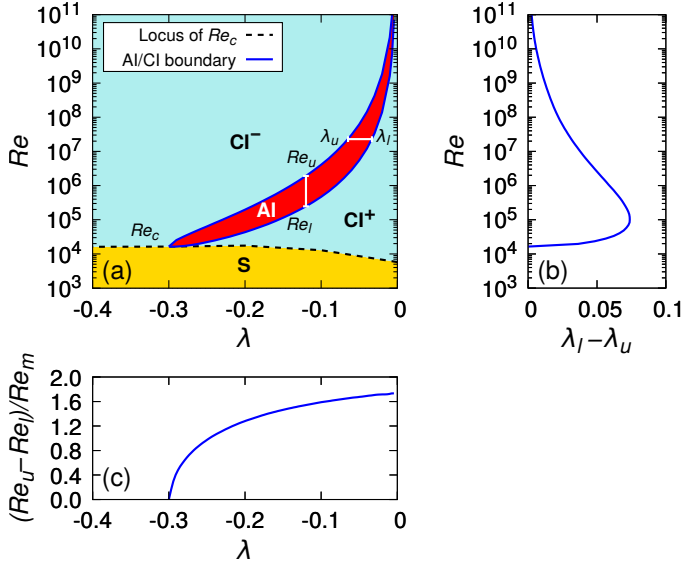


Figure 4: (a) Parametric representation (Re , λ) of the AI/CI instability regions for the CPF. Here S indicates linear stability. (b) The range of λ , ($\lambda_l - \lambda_u$), supporting AI, as a function of Re . (c) The range of Re , $(Re_u - Re_l)/Re_m$, supporting AI as a function of λ ; here $Re_m = (Re_u + Re_l)/2$. Note that Re_u and Re_l are not relevant for $\lambda = 0$, which exhibits CI^+ for all Re (Deissler 1987).

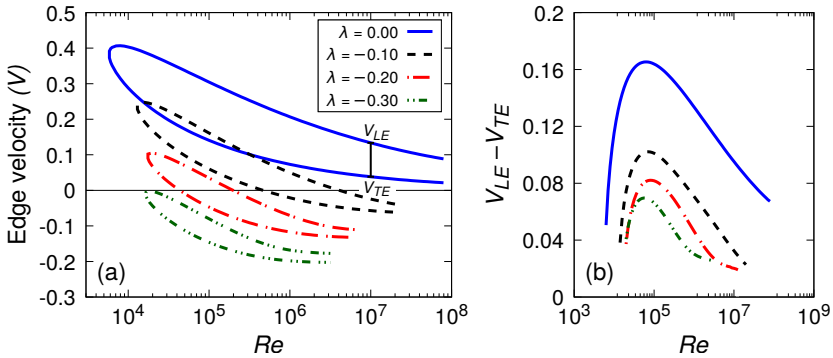


Figure 5: (a) Leading (V_{LE}) and trailing edge (V_{TE}) velocities of the disturbance wave packet as a function of Re . (b) Wave-packet dispersion, $V_{LE} - V_{TE}$, as a function of Re .

determine the range of V ($= x/t$) for which the wave packet shows temporal growth. The two rays where this growth rate is zero correspond to leading and trailing edges of the amplifying wave packet; see also Huerre & Rossi (1998).

The variation with Re of leading and trailing edge velocities (V_{LE} and V_{TE} respectively) for the CPF is plotted in figure 5(a). We see that V_{TE} decreases monotonically with Re for all λ (≤ 0), implying that viscosity has a stabilizing effect on the onset of AI, i.e., a decrease in Re makes it harder for the flow to reach the critical condition for absolute instability. A similar observation has been reported earlier in the context of a wake (Monkewitz 1988) and a separated boundary layer (Avanci *et al.* 2019). Interestingly, $V_{TE} \rightarrow 0$ as $Re \rightarrow \infty$ for $\lambda = 0$,

implying that the PPF is on the verge of becoming absolutely unstable for asymptotically large Re (although it is never realized) and therefore, at these values of Re , a slight negative plate speed can make the flow absolutely unstable, as seen in figure 4(a). Furthermore, V_{LE} also decreases monotonically with Re . (This was observed by Deissler (1987) for PPF at lower values of Re but he did not calculate V_{LE} for large Re as done presently.) As a result, a further small increase in the negative plate speed can make V_{LE} negative for sufficiently large Re . This would make the wave packet switch the direction of propagation and move opposite to the bulk motion. As Re decreases, higher values of negative λ are necessary to bring V_{TE} and V_{LE} down to zero and make them negative (figure 5a). Thus the main reason for the switch from AI back to CI (or to CI^-) is the significant decrease in V_{LE} with Re , which facilitates an upstream propagation of the wave packet for a certain range of negative plate speeds. The peculiar behaviour of V_{TE} and V_{LE} seen in figure 5(a) is what is responsible for the $CI^+ \rightarrow AI \rightarrow CI^-$ transitions observed for the CPF for $-0.2924 < \lambda < 0$.

The difference between V_{LE} and V_{TE} , which is a measure of the degree of dispersion of the wave packet is shown in figure 5(b). For a given λ , the dispersion first increases with Re , reaches a maximum and thereafter decreases. As a result, for Reynolds numbers corresponding to large dispersion, the AI can be expected to be present for a larger range in λ , i.e., more negative values of λ will be needed to transform AI into CI^- . This is evident from figure 4(b), which shows that the range $\lambda_l - \lambda_u$ for which AI exists first increases with Re and then decreases. These results are useful in understanding the role played by viscosity in *sustaining* absolute instability in the CPF. It appears that viscosity plays a “dual” role in this regard - for moderately large Re (corresponding to large wave-packet dispersion; figure 5b), viscosity sustains AI for a larger range of negative λ (or “promotes” its sustenance; figure 4b), whereas for low and high Re , AI is realized over a narrower range of λ (implying that viscosity “suppresses” the sustenance of AI). This behaviour is qualitatively similar to the dual role of viscosity in making the flow unstable in the first place, i.e., the viscous mechanism promotes disturbance amplification only for intermediate values of $Re (> Re_c)$, and the instability gets progressively weaker as $Re \rightarrow \infty$ (Drazin & Reid 2004). Note that the shapes of the edge velocity curves in figure 5(a) are strikingly similar to those of the neutral curves for the primary instability of CPF (Potter 1966; Kirthy K. & Diwan 2021). Incidentally, for a fixed Re , the wave packet dispersion decreases monotonically as λ becomes more negative (figure 5b). This is reflected in a monotonic decrease in the range of Re (i.e., $Re_u - Re_l$) for the realization of AI, as λ is decreased from zero; see figure 4(c).

2.3. Choice of an “objective” frame of reference for AI/CI distinction

At this point, it is pertinent to ask whether there exists an “objective” laboratory frame of reference for distinguishing between CI and AI for the CPF, as it is a strictly parallel flow. In other words, would the distinction between CI^+ , AI and CI^- disappear, if the observer moved with a conveniently-chosen frame of reference? As discussed in Huerre & Rossi (1998), for a weakly non-parallel flow or for a flow which is continuously forced at a certain location, the laboratory frame of reference is well defined as the streamwise invariance is broken. On the other hand, strictly parallel flows such as the PPF and CPF are invariant with respect to translation in x , but the introduction of viscosity requires the no-slip condition to be satisfied, and therefore the laboratory frame of reference for these flows is unambiguously defined. This may be interpreted as the PPF and CPF not being *Galilean invariant* (Huerre & Rossi 1998), in the sense that any change in the observer frame of reference necessitates the plate velocities to be appropriately changed to satisfy the no-slip condition in the new frame.

To illustrate this point further, we carry out the following exercise. We consider $\lambda < 0$, with the upper plate moving in the negative x direction (supplementary figure S4a), which exhibits CI^- for a range of Re (figures 1c and 3). Suppose the observer moves with a reference frame

fixed to the upper plate. This makes the lower plate move in the positive x direction, resulting in $\lambda > 0$ in the moving frame of reference, with $|\lambda|$ remaining constant (supplementary figures S4b and S4c). As a result of this change in reference frame, the wave-packet edge velocities are shifted by an amount $+|\lambda|$ and the CI^- appears to transform into CI^+ ; see supplementary figure S4(d) for a specific case of $\lambda = -0.25$. (A similar shift in the edge velocities in a moving frame is also seen for the PPF; supplementary figure S5). However, it is important to note that the character of the base flow has changed from $\lambda = -0.25$ in the stationary frame to $\lambda = +0.25$ in the moving frame, and we do not expect CI^- to be present for the latter case since $\lambda > 0$ (figure 1b). Furthermore, there are important differences in the stability characteristics of the CPF between $\lambda < 0$ and $\lambda > 0$, with regard to the behaviour of the saddle point (supplementary figure S3) as well as that of the temporal eigenvalues (Kirthy K. & Diwan 2021). In summary, an ‘‘objective’’ (or the laboratory) reference frame for the CPF for $\lambda < 0$ ($\lambda > 0$), is any frame in which one of the plates is stationary and the other moves in the opposite (same) direction to the bulk flow. We impose the condition of ‘‘zero group velocity’’ (for determining the saddle point) in this frame of reference for making the AI/CI distinction. If $\lambda < 0$, CI^- (as well as AI for $\lambda \in (-0.2924, 0)$) is manifested, whereas, if $\lambda > 0$, only CI^+ is manifested.

3. Comparison with Ginzburg-Landau framework

The $CI^+ \rightarrow AI \rightarrow CI^-$ transitions for the CPF can be well understood in terms of the Ginzburg-Landau (G-L) framework. Towards this, we use a slightly modified form of the G-L equation given by

$$\frac{\partial \Psi}{\partial t} + \tilde{U} \frac{\partial \Psi}{\partial x} = \mu \Psi + \kappa \frac{\partial^2 \Psi}{\partial x^2}, \quad (3.1)$$

where $\Psi(x, t)$ is the disturbance amplitude, \tilde{U} is velocity, and κ is a new parameter introduced to mimic kinematic viscosity in the O-S equation; $\kappa = 1$ results in the classical G-L equation (Huerre & Monkewitz 1990). Note that μ in (3.1) does not represent dynamic viscosity but is a measure of disturbance growth. Introducing $\Psi = \hat{\Psi} e^{i(\alpha x - \omega t)}$ into (3.1) and applying the Briggs-Bers criterion gives us the condition for AI as $\mu > \tilde{U}^2 / (4\kappa)$.

In (3.1), μ has the dimensions of velocity gradient and κ that of kinematic viscosity. We find it convenient to choose a velocity scale as μL and define a Reynolds number given by

$$\tilde{Re} = \frac{\mu L^2}{\kappa}, \quad (3.2)$$

where L is the length scale used to non-dimensionalize x in (3.1), assumed fixed for the present purposes. Note that \tilde{U} could have also been chosen as a velocity scale for defining \tilde{Re} but we prefer to use it as a free parameter. We consider \tilde{Re} and \tilde{U} to be respectively equivalent to Re and λ in the CPF analysis. For enabling comparison, the AI/CI boundary for the CPF on the $Re - \lambda$ plane in figure 4(a) is re-plotted in figure 6(a) in a different representation.

Next we construct the AI/CI boundary in the $\tilde{Re} - \tilde{U}$ space for the modified G-L equation, which we do in two different ways. First, we keep κ constant so that $\tilde{Re} \propto \mu$ (3.2) and the dividing AI/CI boundary scales as $\tilde{Re} \propto \tilde{U}^2$ (figure 6b). Secondly, μ is held constant so that $\tilde{Re} \propto (1/\kappa)$ and the dividing boundary in this case is given by $\tilde{Re} \propto (1/\tilde{U}^2)$ (figure 6c). It is evident that the first case corresponds to region ‘‘A’’ of the dividing boundary for the CPF (figure 6a) where viscosity suppresses the sustenance of AI, whereas the second case corresponds to region ‘‘B’’ where viscosity promotes the sustenance of AI (by enhancing dispersion as Re decreases; figure 5b). Furthermore, the CI region for the G-L equation is

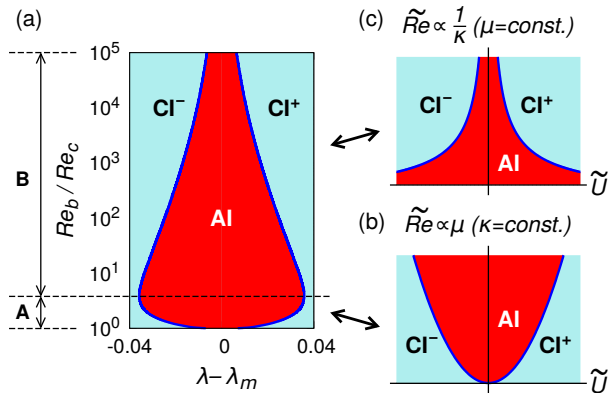


Figure 6: (a) The boundary dividing AI and CI in figure 4(a) represented as Re_b/Re_c as a function of $\lambda - \lambda_m$, where Re_b denotes the Reynolds number corresponding to the dividing boundary and can be either Re_l or Re_u , and $\lambda_m = (\lambda_l + \lambda_u)/2$. (b) and (c) The dividing boundary between AI and CI in the $\tilde{Re} - \tilde{U}$ space for the G-L equation (3.1), with κ and μ held constant respectively.

divided into $CI^+(\tilde{U} > 0)$ and $CI^-(\tilde{U} < 0)$. This is evident from the sign of the imaginary part of the absolute wavenumber for the G-L equation ($\alpha_s = -\frac{i\tilde{U}}{2\kappa}$) (Huerre & Rossi 1998). When \tilde{U} changes from positive to negative, α_s moves from lower half to upper half in the complex α plane, implying that the wave packet amplifies in the negative x direction; see supplementary figure S6. This analysis shows that the G-L equation reproduces the CI-AI transitions for the CPF (i.e., $CI^+ \rightarrow AI \rightarrow CI^-$) more closely than it does for other common examples, such as a mixing layer or a separated boundary layer, which exhibit only the $CI^+ \rightarrow AI$ transition; the transition from AI to CI^- for these flows has not been reported to our knowledge (see, e.g., Huerre & Monkewitz 1985). This provides a further support to the utility of the G-L equation as a model problem for studying the spatio-temporal instability of fluid flows.

4. Conclusion

We have reported a spatio-temporal stability analysis of the Couette-Poiseuille flow using the Orr-Sommerfeld equation to reveal some remarkable and previously unknown features with regard to the AI/CI behaviour of the CPF, as summarized below.

(i) The CPF is shown to exhibit absolute instability for a range of negative plate speeds, $\lambda \in (-0.2924, 0)$. Even the slightest of negative plate motions is sufficient to trigger AI, provided Re is large enough.

(ii) For a given Re , the CPF undergoes $CI^+ \rightarrow AI \rightarrow CI^-$ transitions, as λ is made progressively more negative. The presence of an “upstream” convective instability (CI^-), i.e., an unstable wave packet moving opposite to the bulk motion, seems to be a unique feature of the CPF not reported previously.

(iii) For $\lambda \in (-0.7, -0.2924)$, the only instability possible for the CPF is the “upstream” convective instability. Neither CI^+ nor AI is realized for these values of λ .

(iv) For the PPF, the leading and trailing edge velocities of the unstable wave packet decrease monotonically with Re , approaching zero as $Re \rightarrow \infty$. It is this feature that enables realization of AI and CI^- for the CPF, even for small negative values of λ .

(v) For a given λ , the wave-packet dispersion first increases with Re , following which it decreases. This reveals a peculiar “dual” role of viscosity in sustaining absolute instability in

the CPF; viscosity promotes sustenance of AI at moderate Reynolds numbers but suppresses it for lower and higher values of Re .

(vi) The $CI^+ \rightarrow AI \rightarrow CI^-$ transitions observed for the CPF are consistent with the Ginzberg-Landau (G-L) framework, which also admits similar transitions. In fact, the CPF exemplifies the G-L model better than other known examples of linearly unstable flows.

We expect some of these results to be applicable to other non-inflectional flows, governed by viscous mechanism, that might become absolutely unstable. This can potentially open up new directions of research in understanding the role of viscosity in triggering and sustaining absolute instability in shear flows.

Acknowledgements. The authors thank Dr. Abhijit Mitra from Israel Institute of Technology, Technion, for lending his stability code. Thanks are due to Prof O. N. Ramesh from IISc, Bengaluru, for useful discussions.

Funding. SSD acknowledges financial support from IISc, Bengaluru as a start-up grant (No. 1205010620).

Declaration of interests. The authors report no conflict of interest.

REFERENCES

- ALAM, M. & SANDHAM, N. D. 2000 Direct numerical simulation of ‘short’ laminar separation bubbles with turbulent reattachment. *J. Fluid Mech.* **410**, 1—28.
- AVANCI, MATEUS P., RODRIGUEZ, DANIEL & DE B. ALVES, LEONARDO S. 2019 A geometrical criterion for absolute instability in separated boundary layers. *Phys. Fluids* **31**, 014103.
- BRIGGS, RICHARD J 1964 Electron-stream interaction with plasmas. *Monograph MIT, Cambridge USA* (29).
- CHOMAZ, JEAN-MARC 2005 Global instabilities in spatially developing flows: non-normality and nonlinearity. *Annu. Rev. Fluid Mech.* **37**, 357–392.
- COWLEY, SJ & SMITH, FT 1985 On the stability of Poiseuille–Couette flow: a bifurcation from infinity. *J. Fluid Mech.* **156**, 83–100.
- DEISSLER, ROBERT J 1987 The convective nature of instability in plane Poiseuille flow. *Phys. Fluids* **30** (8), 2303–2305.
- DRAZIN, PHILIP G & REID, WILLIAM HILL 2004 *Hydrodynamic stability*. Cambridge university press.
- GOVINDARAJAN, R & SAHU, KC 2014 Instabilities in viscosity-stratified flow. *Annu. Rev. Fluid Mech.* **46**, 331–353.
- HUERRE, PATRICK & MONKEWITZ, PETER A 1985 Absolute and convective instabilities in free shear layers. *J. Fluid Mech.* **159**, 151–168.
- HUERRE, PATRICK & MONKEWITZ, PETER A 1990 Local and global instabilities in spatially developing flows. *Annu. Rev. Fluid Mech.* **22** (1), 473–537.
- HUERRE, P & ROSSI, M 1998 Hydrodynamic instabilities in open flow. In *Hydrodynamics and nonlinear instabilities* (ed. Godreche C & Manneville P). Cambridge University Press.
- KIRTHY K., SRINIVAS & DIWAN, SOURABH S. 2021 Energy budget analysis and neutral curve characteristics for the linear instability of Couette–Poiseuille flow. *Phys. Fluids* **33**, 034102.
- KLOTZ, LUKASZ, LEMOULT, GRÉGOIRE, FRONTZAK, IDALIA, TUCKERMAN, LAURETTE S & WESFREID, JOSÉ EDUARDO 2017 Couette–Poiseuille flow experiment with zero mean advection velocity: Subcritical transition to turbulence. *Phys. Rev. Fluids* **2** (4), 043904.
- KUMAR, R. & WALTON, A. 2019 Self-sustaining dual critical layer states in plane Poiseuille–Couette flow at large Reynolds number. *Proc. R. Soc. A* **475**, 20180881.
- LINGWOOD, R. J. 1995 Absolute instability of the boundary layer on a rotating disk. *J. Fluid Mech.* **299**, 17–33.
- MONKEWITZ, PETER A 1988 The absolute and convective nature of instability in two-dimensional wakes at low Reynolds numbers. *Phys. Fluids* **31** (5), 999–1006.
- NISHIOKA, M, ICHIKAWA, Y & OTHERS 1975 An experimental investigation of the stability of plane Poiseuille flow. *J. Fluid Mech.* **72** (4), 731–751.
- OLENDRARU, C. & SELIER, A. 2002 Viscous effects in the absolute-convective instability of the Batchelor vortex. *J. Fluid Mech.* **459**, 371–396.
- POTTER, MERLE C 1966 Stability of plane Couette–Poiseuille flow. *J. Fluid Mech.* **24** (3), 609–619.
- SCHMID, PETER J & HENNINGSON, DAN S 2012 *Stability and transition in shear flows*, vol. 142. Springer Science & Business Media.